



Comparative seismic performance assessment of RC and RC/ECC hybrid frame structures: a shake table study

Fasih Ahmed Khan¹ · Muhammad Rashid¹ · Sajjad Wali Khan¹ · Muhammad Rizwan¹ · Yasir Irfan Badrashi¹ · Muhammad Fahim¹ · Muhammad Ashraf Tanoli² · Wasim Khaliq³ · Akhtar Gul¹

Received: 28 August 2021 / Accepted: 29 October 2021 / Published online: 13 November 2021
© Springer Nature Switzerland AG 2021

Abstract

This study focuses on the efficient utilization of engineered cementitious composite (ECC) in reinforced concrete (RC) frame structures. In this regard, ECC has been incorporated in the joint panel and plastic hinge zones of the connecting frame elements. For the evaluation of dynamic performance assessment of such hybrid ECC-RC frame structure, a two-story (low rise) RC-frame structure was selected. Two different structural detailing configurations were considered, a model confirming modern seismic code requirements (Code-Compliant Models), while the other was detailed with some seismic code deficiencies (Non-Compliant Models). For experimental testing, 1:3 reduced scale representative models were fabricated. These models were subjected to a 1994 Northridge accelerogram record through a unidirectional shake table. The damage observed in the conventional RC model has exhibited diagonal cracking at the joint panel and concrete crushing. In contrast, ECC-RC models demonstrated minor column damages without severe cracking of the joint core. For dynamic response evaluation, the seismic response parameters (yield stiffness, yield strength, ductility, overstrength factor, and R-factor) for all the models were computed and compared to evaluate the possibility of incorporating ECC at crucial locations. For the ECC enhanced code-compliant and non-compliant models, the response modification factor increased by 37.62% and 16.61%, respectively, compared to the RC countermodels. In addition, the peak input acceleration was correlated with the peak roof displacement to obtain the seismic response envelopes. The performance of ECC-RC models was exceptional for the non-compliant models, which enhance the seismic ductility and energy dissipation for highly optimized frame structures. Hence, it is believed that the efficient use of ECC in critical regions of frame structures can be vital in mitigating the seismic risk.

Keywords Shake table · Joint damages · ECC · Response modification factor · Seismic performance · Ductility

✉ Fasih Ahmed Khan
fasiahmad@uetpeshawar.edu.pk

Muhammad Rashid
mrashidad@gmail.com

Sajjad Wali Khan
drsajjadwalikhan@uetpeshawar.edu.pk

Muhammad Rizwan
mrizwan@uetpeshawar.edu.pk

Yasir Irfan Badrashi
yasir_badrashi@uetpeshawar.edu.pk

Muhammad Fahim
drfahim@uetpeshawar.edu.pk

Muhammad Ashraf Tanoli
matanoli@giki.edu.pk

Wasim Khaliq
wasimkhaliq@nice.nust.edu.pk

Akhtar Gul
akhtarwazir@uetpeshawar.edu.pk

¹ Department of Civil Engineering, University of Engineering & Technology, Peshawar, Pakistan

² Department of Civil Engineering, GIK Institute, Topi, Pakistan

³ National University of Sciences and Technology (NUST), NUST Campus, Sector H-12, Islamabad, Pakistan

Introduction

Moment-resisting frame structures are most widely adopted for low-rise buildings in high tectonic regions. However, the serviceability of the frame structures gets compromised by the poor performance of beam-column joints during severe ground shaking [1]. Strong earthquakes impose a greater shear demand on beam-column joints, making them more delicate components in frame structures [2]. The recently observed earthquake evidence shows that the critical part of the structural system most often failed brittle with diagonal cracks in the joint panels [3]. For RC frame structures, building codes provide guidelines for appropriate reinforcement in beam-column joint regions. Under lateral load demand, the framing elements are expected to carry and maintain substantial plastic deformations without undergoing any severe damages. The recent field studies after Chile (2010) and New Zealand (2010) earthquakes demonstrated that the structures designed based on current seismic codes performed better in achieving the life safety level; however, the resultant economic impacts were enormous [4, 5].

A field study revealed that the main reasons for structural joint failure in many developing countries are poor construction practices like sub-standard concrete, a reduced ratio of reinforcement, lack of shear hoops in joint zones, and practicing 90° shear hooks [6]. The structural joints encounter multi-directional shear stresses during lateral loading, making the structure component more vulnerable [7].

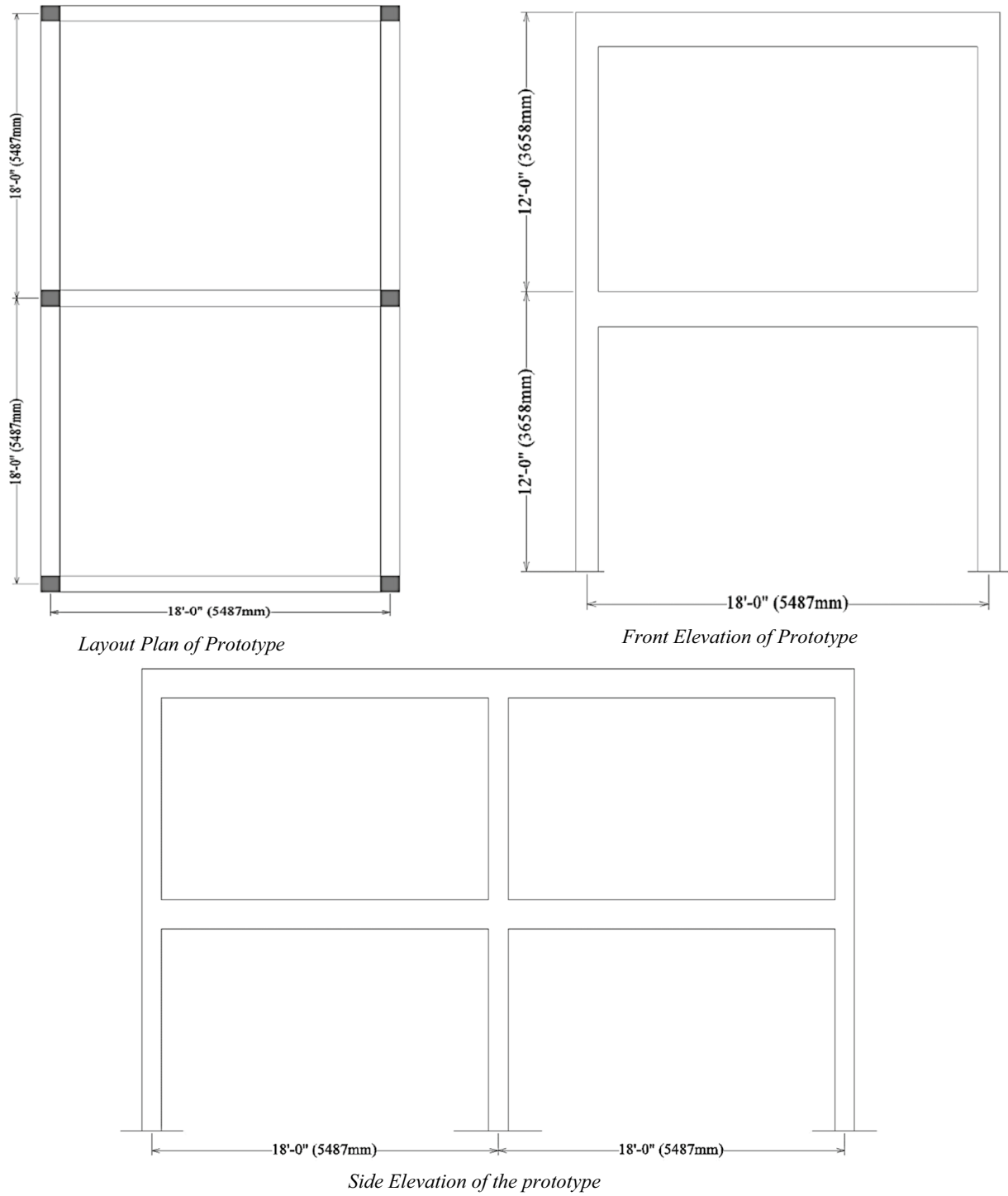
The RC structure seismic capacity is improved by providing additional reinforcement in the critical region of the structure, which provides enough confinement to the core material and hence improves the structural joint shear capacity. The ACI-ASCE committee 352 highly recommends that the structural detailing be sufficient in terms of confinement and detailing to avoid severe diagonal crack formations at the joint cores [8]. The resultant flexibility of the structural system gets improved with sufficient confining of the joints. However, following these guidelines usually results in reinforcement congestion, which results in construction problems such as concrete pouring and compaction, making the joint regions more fragile during lateral loading to maintain the designed level deformation [9]. Furthermore, significant flexural cracking and joint zone damage have been observed due to lateral load less than design demand low-strength concrete frames, which can cause shear cracks at the local level and contribute to soft story formation globally [10].

In addition to the amount and arrangement of reinforcement used for strengthening the joint areas, other studies have focused on using enhanced quality materials such as

fiber-reinforced composites and high-performance fiber reinforced concrete (HPFRC) [11–14] in the joint regions for the improvement of structural performance. The newly developed fiber-based composite materials offer many emerging research topics in civil engineering industries [15–18]. High-performance concrete is more expensive than ordinary concrete, but this drawback can be compensated for by its improved response and lower unit weight. Liu et al. [19] studied high-strength concrete (HSC); the results showed that HSC members failed in a very brittle manner in the anchorage zone and significantly weakened the beam reinforcement bond in the joint zones. However, this drawback was overpowered by introducing fibers into the matrix. With the introduction of the fibers in the concrete matrix, an enhancement in structural ductility was noted, which is crucial in preserving the overall performance of a structural system, especially in improving the energy dissipation and elasticity [20, 21]. Previous studies have shown that fiber-reinforced material exhibits ductile behavior in compression and tension with hardening or softening tensile strain when enough fibers are mixed in concrete [22]. Consequently, the overall response of structure gets improved during lateral dynamic loading. The capability to sustain and resist significant plastic deformation due to shear reversals during seismic activity is another considerable requirement that has been met by the fiber-reinforced materials [2].

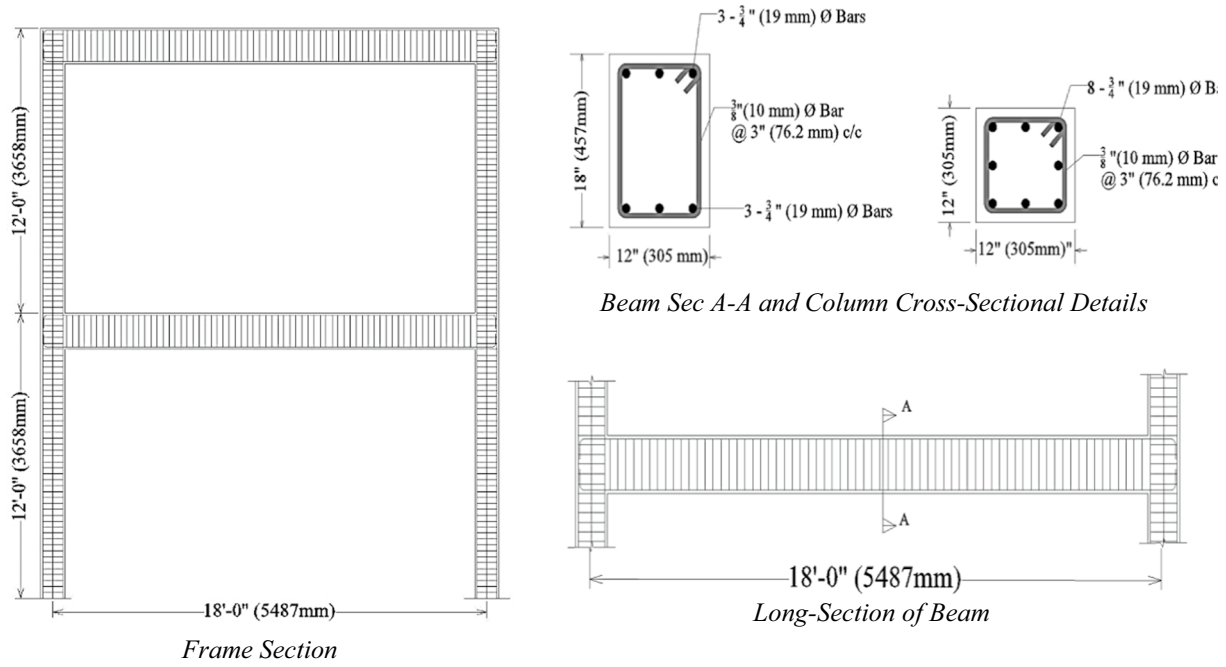
ECC is a class of high-performance fiber-reinforced concrete (HPFRC) with inherent high tensile and shear straining capacities [23, 24]. Effective use of fiber-reinforced composites at the critical regions of a structural system may improve the seismic behavior of frame structures. Several studies reveal that incorporating fiber-reinforced composites can significantly reduce or remove the shear reinforcement at joints [25]. Shannag et al. [26] study concluded that using steel FRC to replace traditional concrete in beam-column joints would substantially improve seismic behavior. Likewise, some experimental research has shown that ECC use in beam-column joints can significantly enhance the seismic stability of lightly strengthened joints [27, 28].

The literature has explicitly reported that the implementation of code requirements is an issue for practicing engineers. The same has been addressed with the application of high-performance fiber-reinforced concrete (HPFRC) in structural components. However, very little work has been carried out on this topic, and further experimentation is required to check the reliability of HPFRC in the joint region. Within this context, the possible global consequences of using fiber-reinforced concrete in the joint and plastic regions of earthquake-resistant RC frames and comparing the potential behavior with ordinary concrete structures are of significant interest. Therefore, this study focuses on an ambitious investigation conducted through

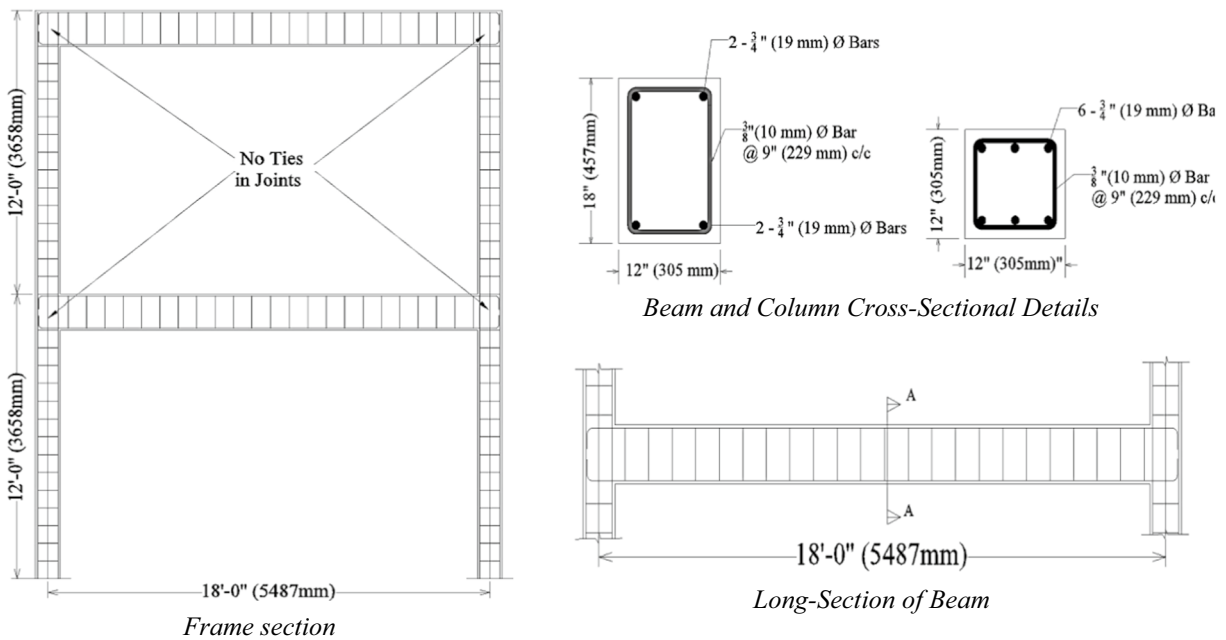


(a) Layout Plan and Elevation of the Prototype Structure

Fig. 1 Plan, geometrical and structural description of the considered prototype



(b) Structural detailing of considered code-compliant frame



(c) Structural detailings of the considered non-code-compliant frame with no ties in joints panel

Fig. 1 (continued)

shake table experiments to describe the seismic response of RC and ECC-RC composite frame structures. Such type of structures is widely used as typical residential and commercial buildings.

Experimental program

Geometrical and structural description of considered models

The geometrical and reinforcement details of the considered prototype two-story frame structure are illustrated in

Fig. 1. It has a symmetrical plan of two-bay by one bay having a bay length and story height of 18-ft (5487 mm) and 12-ft (3658 mm). The structural design was carried out for a high seismic zone with soil type B and PGA of 0.40 g, using a lateral force-based procedure. Four different models were considered for the current study. The classification was based on reinforcement detailing (code compliant and non-compliant) and the use of standard concrete or composite material (ECC) at the structural joints and plastic hinge zones of beams and columns. The structural detailing of the code-compliant models was carried out as per modern seismic building code, where the columns having dimensions of 12-inch × 12-inch (305 mm × 305 mm) were reinforced with 8, #6 (8 × 20 mm) rebars and longitudinal and transverse beams with dimensions 12-inch × 18-inch (305 mm × 457 mm) provided with 6, # 6 (6 × 20 mm) steel rebars and confined with #3 rebars (10 mm) having 135° hooks at 3-inch c/c (76.2 mm c/c). Concrete having 28 days strength of 3000 psi (21 MPa) was used in code-compliant models. For the non-compliant models, the optimization in reinforcement detailing and the material were considered, i.e., the use of lower strength concrete, lack of confining ties at the joint panels, a larger spacing of reinforcement in framing members, a reduced ratio of main reinforcement, and provision of non-seismic hooks in shear hoops. The geometric configuration of the non-compliant models was the same as that of a

Table 2 Mix proportioning for ECC material

ECC mix design for 1 m ³ batch					
Cement, Kg	Sand, Kg	Fly Ash, Kg	Water, Kg	HVWR*, Kg	PVA, Kg
583	467	700	523	32	19

*High volume water-reducing admixture was used having a dosage of 2.5 kg per 100 kg of binding material

code-compliant model with 6, #6 (6 × 20 mm) steel rebars in the column, 4, #6 (4 × 20 mm) steel rebars in beams confined with #3 (10 mm) bars at 9-inch c/c (228.6 mm). Additionally, low-strength concrete of 2000 psi (14 MPa) was used throughout the model construction, and no shear hoops were provided in the joint panels. The structural specifications for the composite frame models are the same as the code-compliant and non-compliant RC models, respectively. Furthermore, the hybrid frame models were cast with ECC incorporation at the core joint and extended on either side of the panel in the connecting beam and columns plastic hinge length (Fig. 4).

The structural description of the selected models is summarized in Table 1. For mass simulation, each model was loaded with 2400 kg additional mass in the form of steel plates secured with the floor slab (Table 2). The mass

Table 1 Characteristic features of the considered models

Model description		RC code compliant	RC code deficient	ECC/RC code compliant	ECC/RC code deficient
Beams (Long and Trans), in (mm)	12 × 18 (304 × 459)	✓	✓	✓	✓
Column, in (mm)	12 × 12 (304 × 304)	✓	✓	✓	✓
Concrete strength, psi (MPa)	3000 (21)	✓	×	✓	×
	2000 (14)	×	✓	×	✓
Steel yield strength, ksi (MPa)	60 ksi (414 MPa)	✓	✓	✓	✓
Main reinforcement	Beam	6, #6 (6, 20 mm)	4, #6 (4, 20 mm)	6, #6 (6, 20 mm)	4 #6 (4, 20 mm)
	Column	8, #6 (8, 20 mm)	6, #6 (6, 20 mm)	8, #6 (8, 20 mm)	6, #6 (6, 20 mm)
Shear reinforcement	Beam	#3 @ 3" c/c (10 mm @ 76 mm)	#3 @ 9" c/c (10 mm @ 229 mm)	#3 @ 3" c/c (10 mm @ 76 mm)	#3 @ 9" c/c (10 mm @ 229 mm)
	Column	#3 @ 3" c/c (10 mm @ 76 mm)	#3 @ 9" c/c (10 mm @ 229 mm)	#3 @ 3" c/c (10 mm @ 76 mm)	#3 @ 9" c/c (10 mm @ 229 mm)
Joint hoops	With ties	✓	×	✓	×
Hoop hook	135°	✓	×	✓	×
ECC at critical regions (Joint and Beam/ Column Plastic Hinge Length)		×	×	✓	✓

Table 3 Conversion scale factors based on similitude requirements for the prototype models

Physical Quantity	Relationship	Scale Factor
Length	$S_L = L_p/L_m$	3
Stress	$S_f = f_p/f_m$	1
Strain	$S_e = \epsilon_p/\epsilon_m$	1
Specific Mass	$S_p = \rho_p/\rho_m$	1
Displacement	$S_d = d_p/d_m = S_L$	3
Force	$S_F = F_p/F_p = S_L^2 S_f$	9
Time	$S_t = t_p/t_m = S_L \sqrt{(S_e S_p/S_f)}$	$3^{0.5}$
Frequency	$S_\Omega = \Omega_p/\Omega_m = 1/S_t$	$(1/3)^{0.5}$
Velocity	$S_v = v_p/v_m = \sqrt{(S_e S_p/S_f)}$	1
Acceleration	$S_a = a_p/a_m = S_f/S_L S_p$	1/3

S_L =Length Scale Factor, L_p =Prototype Length, L_m =Model Length, S_f =Stress Scale Factor, f_p =Prototype stress, f_m =Model stress, S_e =Strain Scale Factor, ϵ_p =Prototype strain, ϵ_m =Model strain, S_p =Specific Mass Scale Factor, ρ_p =Prototype Specific Mass, ρ_m =Model Specific Mass, S_d =Displacement Scale Factor, d_p =Prototype displacement, d_m =Model displacement, S_F =Force Scale Factor, F_p =Prototype Force, F_p =Model Force, S_t =Time Scale Factor, t_p =Prototype Time, t_m =Model Time, S_Ω =Frequency Scale Factor, Ω_p =Prototype frequency, Ω_m =Model Frequency, S_v =Velocity Scale Factor, v_p =Prototype velocity, v_m =Model velocity, S_a =Acceleration Scale Factor, a_p =Prototype Acceleration, a_m =Model Acceleration

simulation and characterization were based on similitude requirements in similar previous studies [29–31].

Preparation of reduced scale representative models

Simple model idealization was used to cast 1:3 scale down representative models without altering the mechanical and stress–strain properties of the materials [32]. All linear dimensions were scaled down using a scale factor of 3 (Table 3). The standard procedure for material mix design by ACI-211 was used to select the appropriate mix proportion. A mix ratio of 1:1.80:1.60 (C: FA: CA) with w/c of 0.48 yields a compressive strength of 3000 psi (21 MPa)

at 28 days, whereas for 2000 psi (14 MPa) concrete, a mix proportion of 1:3.5:2.87 (C: FA: CA) was selected with w/c of 0.80. Similarly, for the hybrid frame models, the mix proportioning of ECC was carried out in several trials. The constituents were proportioned for 1m³ of the mixed batch. High volume water-reducing admixtures were incorporated at the rate of 2.5% by the cumulative weight of cement and flash. The water to binding material ratio employed was 0.41. The optimum amount of polyvinyl alcohol (PVA) fibers was incorporated at the rate of 1.5% by weight of cement plus fly ash. The stress–strain relationship of the normal concrete in comparison to ECC is shown in Fig. 2. The summary of mix proportioning for ECC is illustrated in Table 2.

Initially, to ensure fixed support for the test models, the base pads were cast with standard concrete with 3000 psi (21 MPa) strength, where beam-type reinforcement was provided in a double layer. After gaining sufficient strength, construction of the superstructure was carried out in series. The ECC was monolithically cast within the specified regions with normal concrete in the formwork. The models were covered with moist bags for enough time to ensure proper curing. The fabrication process for test models is summarized in Fig. 3.

The layout of ECC at critical regions

Various researchers worked out the performance assessments of ECC enhanced specimens from structural components to beam-column joints. Said et al. [33] applied ECC in the joint core and the plastic hinge zones of the connecting element. Qudah and Malej [34] worked out the reverse cyclic testing of ECC enhanced specimens, where the ECC was extended on either side of the joint core in the connecting frame elements. Conceptually, when the demand associated with the applied load exceeds the structural capacity, the plastic distortion gets localized at the plastic hinge zones. Plastic hinge zones are critical regions that control the structural performance in load-carrying capacity and deformation

Fig. 2 Stress–strain relationship for concrete and ECC

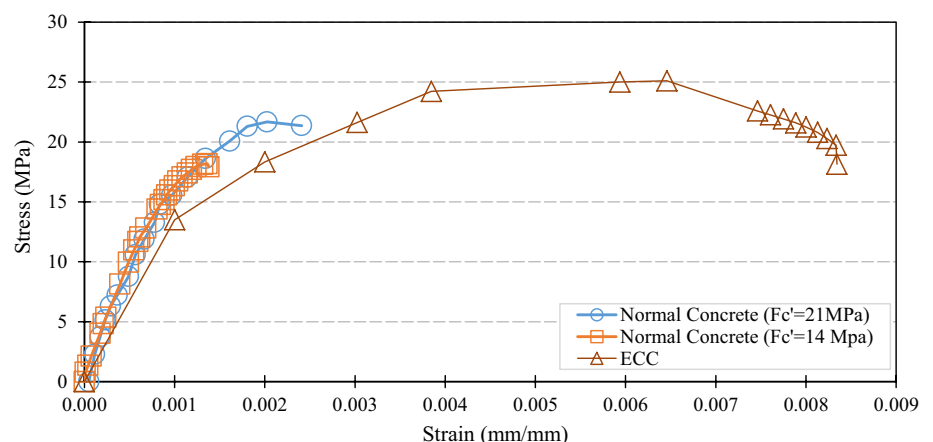




Fig. 3 Fabrication of considered models

[35]. Therefore, the vital areas were cast with ECC for the ECC enhanced models, as shown in Fig. 4.

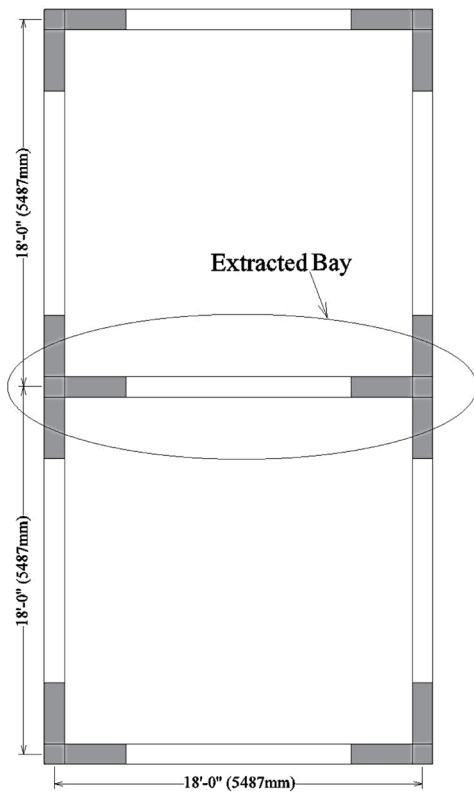
Structural response requisition scheme

During the dynamic excitation, the structure's actual response was captured with the help of several sensors instrumented in the manner shown in Fig. 5. A total of three accelerometers were installed, one at each floor level and one at the base pad level with a capacity of ± 10 g. Additionally, each floor was provided with two linear displacement transducers and one at the base pad level with a capacity of 24

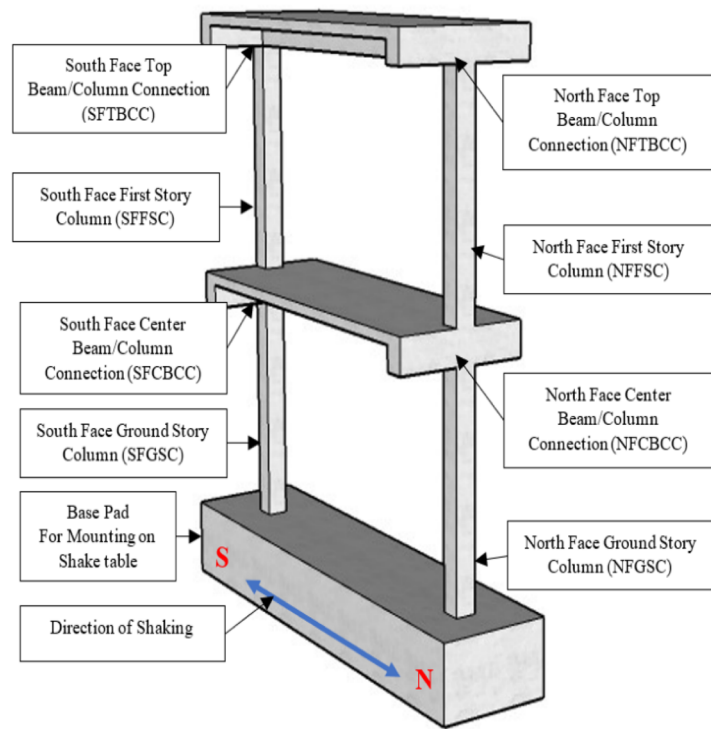
inches. The displacement sensors were mounted on a reference frame to record the relative motion of the frame model.

Base excitation and loading protocol

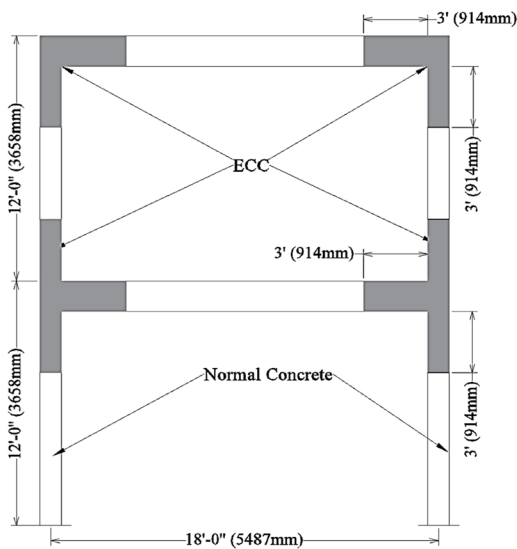
A single degree of freedom actuator was used to excite the test models. The selection of the input time history depends upon many parameters such as shake table capacity and tectonic similarity of the considered regions in the design. The horizontal component of natural accelerogram of 1994 Northridge record, shown in Fig. 6 (Retrieved from the 090 California Department of Mines and Geology



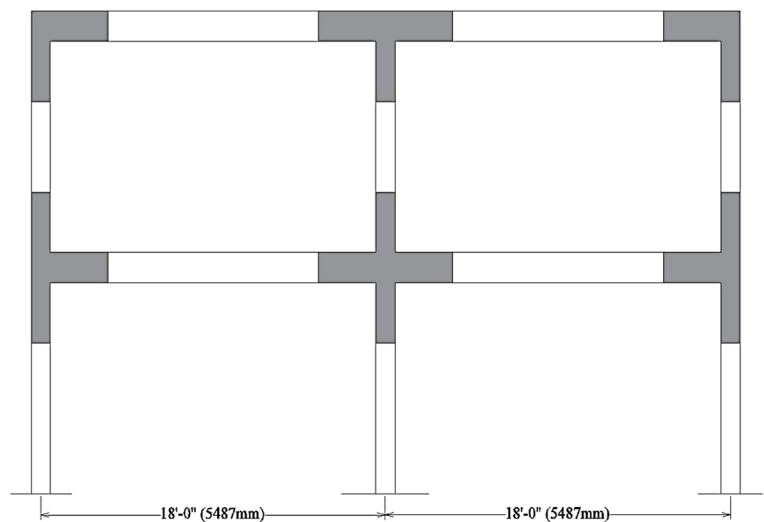
(a) Prototype Layout Plan With ECC



(b) Extracted Middle Frame for Experimental program (Model's Isometric View)



(c) Prototype Front elevation with ECC



(d) Prototype Side view with ECC

Fig. 4 Schematic layout for ECC incorporation at joints and connecting element's plastic hinges zone

(CDMG) Station 24 of 278—Pacific Earthquake Engineering Research (PEER) Center, at the University of California, Berkeley strong motion database) was selected after a

thorough analysis of different time histories. The chosen time history can vibrate the structure with a PGA of 1.0 g,

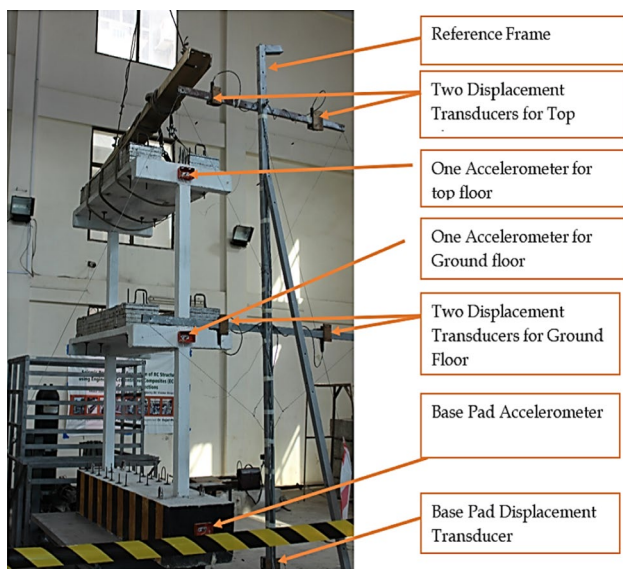
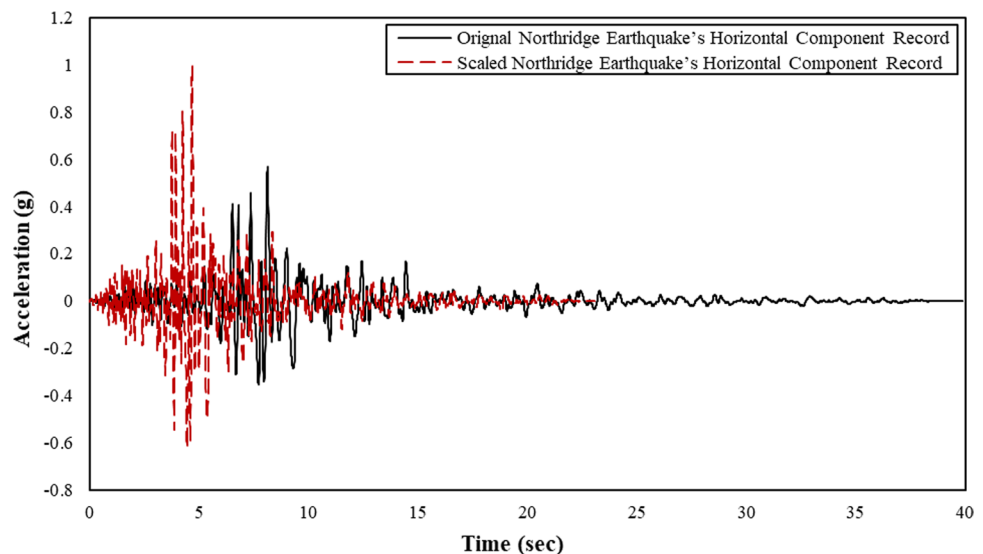


Fig. 5 Instrumentation setup

which is inside the seismic actuator's permissible limits and satisfies the regional seismicity of the selected region.

The selected accelerogram was applied in a series of runs to capture the test frame model's damaging and crack propagation behavior. Each model was subjected to dynamic loading ranging from 5 to 100% of the maximum amplitude of the selected record. The characteristic accelerogram has a PGA, PGV, and PGD of 0.57 g, 518 mm/sec, and 90 mm, respectively. The selected accelerogram was scaled to a PGA of 1.0 g and then applied to each model with 5% to 100% of the maximum amplitude through a seismic actuator; the time step of the selected record was reduced by $1/\sqrt{3}$ while keeping in view the similitude and scaling requirements [36–38].

Fig. 6 Northridge (1994) natural accelerogram applied as input excitation



After each test run, the models were thoroughly investigated for visual cracks and damages. All the models were loaded from elastic to the plastic regime till the incipient collapse state was reached.

Seismic response of the test models

Observed damage mechanism.

ECC/RC code compliant model

Initially, the model was subjected to a self-check run, where the model experienced a PGA of 0.71 g, and vigorous vibration was observed. Tiny flexural cracks appeared at the beam–column interface on both stories. The model underwent a peak roof displacement of 3.62 inches, corresponding to a 1.56% drift ratio. Similarly, during the second run, the model was subjected to a PGA of 0.78 g, yielding a roof drift of 3.25%. The preformed cracks further widened without new cracks formation. The selected accelerogram was applied gradually, scaled from 5 to 80% of actual record intensity. The damage pattern and crack path observed were noted for each test run. Up to 70% runs, no new crack pattern was observed except the degradation associated with the aggravation of existing cracks. In the last run, the model experienced a PGA of 0.63 g with a roof drift ratio of 7.23%. The failure at the ground story column base was observed, where cover spalling and concrete crushing were the primary reasons for the model tilting in out of the plane direction. No ECC spalling and crushing were observed at the structural joints, although the model was at the verge of collapse prevention level (Fig. 7a). It may be attributed to the bridging effect of PVA fibers and the integral nature of ECC material.

Fig. 7 Observed damages at the incipient collapse stage, Refer to Table 3 for damages evaluation

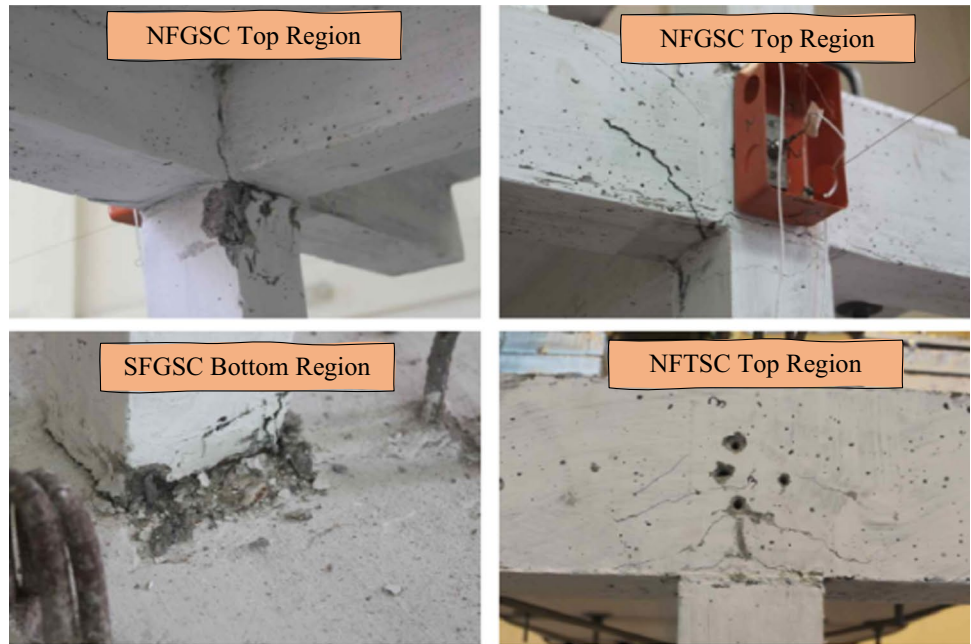


ECC/RC non-compliant model

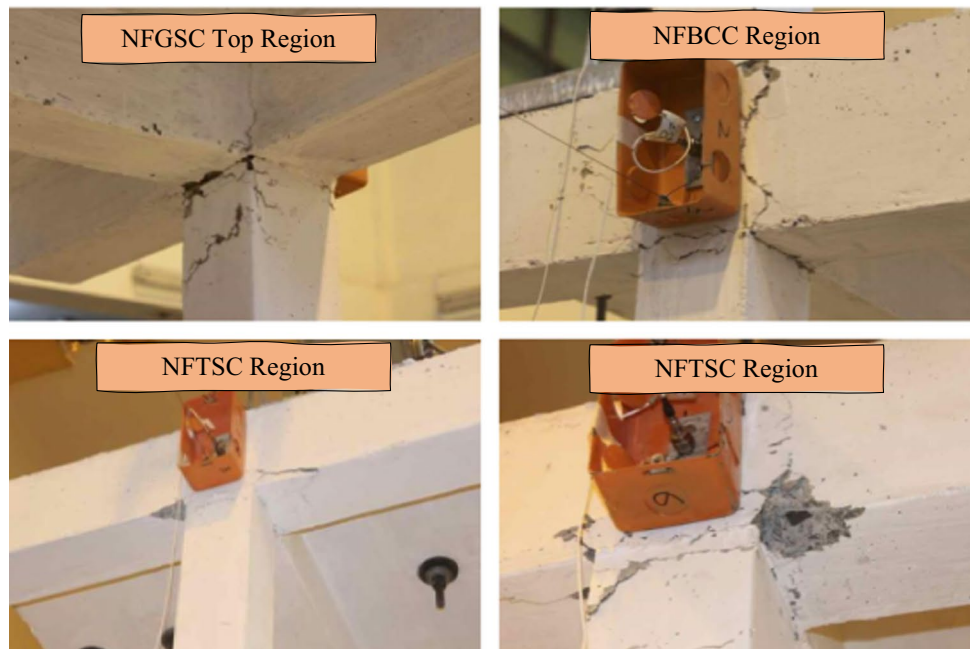
The failure behavior for the optimized model was considerably like the ECC/RC code-compliant model. During self-check, the model experienced a PGA of 0.27 g and underwent a drift ratio of 1.04%. Tiny flexural cracks developed at the end of columns at the ground story (both top and bottom). In the following runs, the existing damages aggravated without new pattern formation. In the final run, the model experienced a PGA of 0.48 g and roof drift of 5.93%,

where tiny hairline dense cracks in the joint were observed at the ground story. The rest of the model joints were safe without any crack formation in the joint core. At the ground story column base, slight column toe crushing and spalling of concrete were observed (Fig. 7b), due to which the model tilted in the out-of-plane direction and hence reached the incipient collapse state.

Fig. 7 (continued)



(c) RC code-compliant model



(d) RC non-compliant model

RC code-compliant model

During self-check excitation, the model experienced a peak roof drift of 0.87%. At the ground story, beams flexure cracks appeared, which can be attributed to the yielding of longitudinal reinforcement in flexure and plastic hinging at the beam's plastic zone. The beam–column interface underwent slight cracking at the ground story due to the main rebars slip mechanism. Flexural cracks were also observed in the ground story column base. In the final run, the model

experienced a PGA of 1.06 g with a peak roof drift ratio of 5.26%. Due to great demand on the external concrete cover in terms of compressive strain during this run, the column base and top at the ground story underwent concrete crushing and cover splitting. Slight cover spalling was also noted at the top story column base (Fig. 7c). Severe crisscross-type cracking of the joint cores at the ground story was noted due to higher moment demand concentration, leading the model to collapse level. It illustrates that the beam plastic hinge

length possesses a higher moment-resisting capacity than the joint yielding capacity.

RC non-compliant model

During the self-check run, the model experienced a peaked roof drift ratio of 0.36%, where slight flexural cracking at the ground and top story columns was observed at both ends of the ground story. Hairline cracking was also observed at the beam ends. In the following runs, no new cracks developed, and the existing cracks were further aggravated. In the final run having a PGA of 0.47 g, the model underwent a peak roof drift ratio of 3.92%. Cover spalling and crushing of concrete at column ends were observed in both stories. Significant vertical cracks appeared at the beam–column interface on the ground story. Additionally, both stories' joint panels exhibit brittle diagonal cracking and a bat-like concrete chunk detached from the top joint (Fig. 7d). The comparative damage evaluations are presented in Table 4 for all the considered models.

Assessment of structural dynamic response

Lateral load-deformation capacity envelops the frame models.

The response data were scaled and transformed for prototype structures according to the similitude requirements. The peak response in each exciting run and the corresponding roof drift were computed. For base shear forces, the cumulative inertial forces associated with each floor mass were calculated and summed. The lateral force–displacement curve was obtained for each model by joining the points corresponding to maximum base shear and the associated roof drift for each test run, as shown in Fig. 8.

The actual response curve was idealized as a bilinear curve using the equal energy principle to calculate different response parameters. The initial slope of the idealized curve is kept similar to the actual curve, and the actual peak displacement observed was taken as the ultimate displacement value. The bilinearization was carried out using iterative procedures, i.e., to equalize the area under the curves. With the incorporation of ECC, the structural yield stiffness and ductility improved. The change in yield strength, yield stiffness, and ductility factor are illustrated in Fig. 9.

Response modification factor (R-factor)

The elastoplastic behavior of frame models can be described in terms of response modification factor (R-Factor). Once

the bilinear capacity curves of the structures are formulated, the R -factor can be calculated from the following relation,

$$R = \frac{V_e}{V_s} = \frac{V_e}{V_y} \times \frac{V_y}{V_s} = R_\mu \times R_s \quad (1)$$

where V_e , V_s and V_y represent the elastic force in the corresponding flexible system, design base shear force, and yielding force in the elastoplastic system. R_s is known as the overstrength-dependent factor, obtained experimentally from dividing the yield force by design base shear force. For ductility dependent factor R_μ , empirical equations are proposed by Newmark and Hall [39, 40] as a function of the structural time period, given as:

$$R_\mu = 1, \text{ for } T < 0.20 \text{ sec} \quad (2)$$

$$\text{or } 0.20 \text{ sec} < T < 0.50 \text{ sec} \quad (3)$$

$$R_\mu = \mu, \text{ for } T > 0.50 \text{ sec} \quad (4)$$

where T represents the elastic time period of a structural system. The summary of the calculation of parameters required for the response modification factor is reported in Table 5. RC frame models underwent a sway type failure mechanism with plastic hinges at the beam ends, with a crack extending to the joint panels. Contrary, the ECC enhanced model showed a column mechanism, where the plastic hinging was observed at the top ends of the column. Furthermore, hairline cracks extended toward the long beam spread in the plastic hinge zone without cracking the joint panels. Compared with the code recommended value of $R = 5$, the R -factor obtained was 50% greater for the RC code-compliant model, which increased by 140% for the ECC counterpart model. This relatively high difference is attributed to the elasticity and confinement of ECC material.

Similarly, for the non-compliant model, the R -factor of ECC-RC differs by 24%, showing a relatively higher energy absorbance capacity of the ECC enhanced model. The high drop in R -factor value for the non-compliant models is due to low standard concrete, reduced shear, main reinforcement ratio, and lack of confining reinforcement at the joint panels. Overall, the ECC enhanced model response was entirely satisfactory in comparison to standard concrete models.

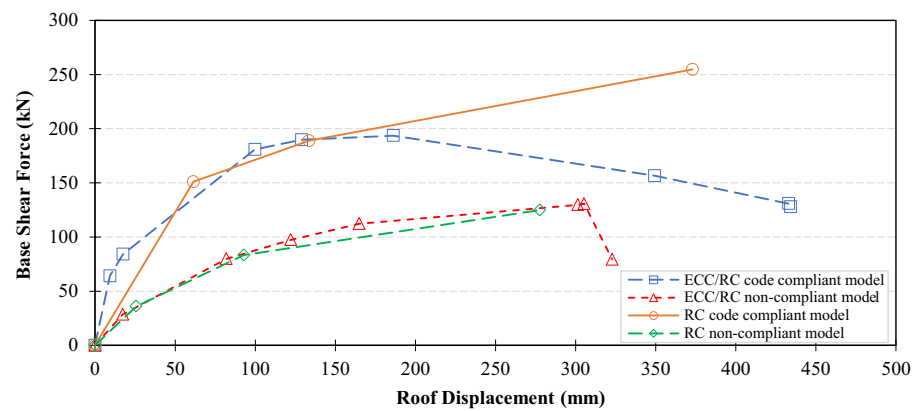
Seismic response curves for the prototype frames

The seismic response curves are helpful for structural response analysis and fragility functions calculation. For each considered model, the seismic response envelops plotted by correlating the model base pad acceleration as PGA with the peak roof displacement of structures. Unlike the

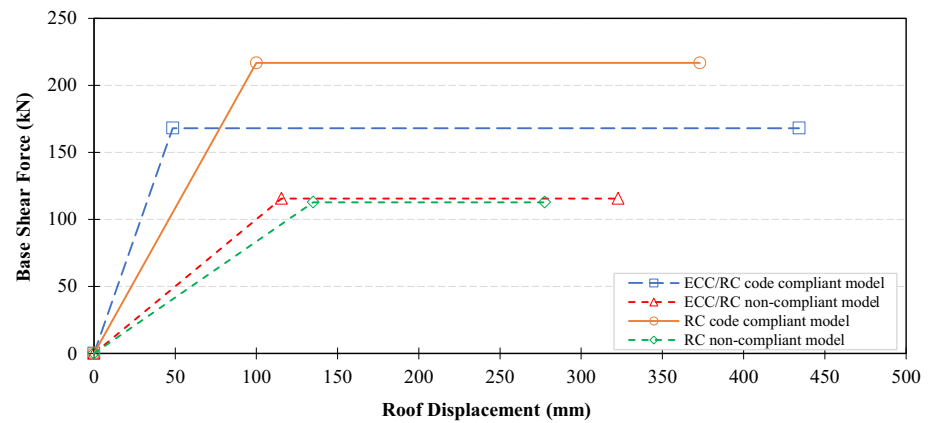
Table 4 Models' comparison and damages evaluation

Model	PGA, (g)	Peak displacement in (mm)	Drift ratio (%)	Base shear kips (KN)	Observations
ECC/RC code complaint	0.71	3.62 (91.95)	1.56	27.50 (122.33)	Flexural cracking at the top and bottom of first story column Hairline cracking at the base of the column on the ground story Flexural cracking at the top of the ground story columns
	0.56	11.45 (290.83)	4.94	33.40 (148.58)	The existing cracks at the beam–column interface aggravated without new cracks path
	0.63	17.26 (438.40)	7.23	35.18 (156.50)	The opening and closing of the interface cracks become visible Concrete spalling at the toe of ground story columns Out-of-plane model tilting was observed Hairline cracks appeared in the transverse beam plastic hinge length zone
ECC/RC non-compliant	0.27	2.44 (62.11)	1.04	12.33 (54.85)	Slight horizontal Flexural cracks at the top and base of the column–beam interface at the top story Slight flexural cracks at the top of the ground story column
	0.49	7.48 (190.12)	3.67	25.23 (112.26)	The aggravation of existing cracks was observed
	0.48	12.83 (325.96)	5.93	29.38 (130.72)	The joints core cracks formation at the ground story joints was observed The ground story both column base cracking at the plastic hinge zone The top story beam–column interface opened completely Hairline cracks at the top story joint zone were observed Concrete crushing at the base of the ground story column was observed
RC code compliant	0.59	2.42 (2.42)	0.87	33.96 (151.06)	Flexural cracking at the beam ends on both stories Flexural cracking at the base of the column on both stories
	0.49	5.26 (133.60)	1.88	42.47 (188.91)	No significant change was observed in crack formation and aggravation
	1.06	14.69 (373.13)	5.26	57.27 (254.74)	Significant widening of existing cracks Cover spalling and crushing at the column base on the ground story Severe x type cracking at the joint panels on the ground story
RC non-compliant	0.10	1.01 (25.65)	0.36	8.08 (35.94)	Minor flexural cracking at the top and bottom of the columns on both story's Flexural cracking at the plastic hinge zones of the longitudinal beam at ground story
	0.20	3.66 (92.96)	1.31	18.73 (83.31)	Further aggravation of existing cracks was observed
	0.47	10.93 (277.62)	3.92	28.07 (124.86)	Concrete crushing and spalling at the top ends of columns on both story's Significant vertical cracks get appeared at the plastic hinge zone of the ground story beam Deep x type cracks developed at the joint panels on both stories A bat-like concrete chunk detached from the top joint panel

Fig. 8 Lateral load-deformation envelopes for the considered prototype structures



(a) Actual curves



(b) Bi-linearized curves

lateral load-deformation envelopes, a clear trend in response cannot be noted due to the high degree of sensitivity of input PGA to the high-frequency noise. From Fig. 9, at the nascent collapse level, the RC code-compliant model can resist the high demand of input PGA (1.06 g). A distinct increase in roof displacement can be observed at the ECC enhanced code-compliant model at the collapse stage. For the non-compliant model, the response of the ECC enhanced model is comparatively better than the RC counterpart in terms of input PGA and peak roof displacement. Incorporating the ECC in the joints and beam/column hinge length had a ductile impact on the displacement ductility of the structure. The ECC structure shows a linear trend up to a PGA of 0.47 g, after which a more significant displacement can be observed (Fig. 10).

Conclusions

This study's following conclusions have been drawn to evaluate the seismic performance of RC and ECC-RC moment-resisting frames.

1. The efficient utilization of ECC in frame structures at the critical regions significantly improves the stiffness and post-yielding behavior of structures located in high seismic zones.
2. In the RC code-deficient models, the cracking mechanism shift from beam failure to column and joint failure. Still, the confinement and bridging effect at the joint panels can significantly improve compliant and non-compliant structures with ECC.
3. The ill effect associated with the brittle failure of concrete in joint cores can be mitigated effectively by incorporating ECC in critical and plastic hinge zones. It was observed that the ECC region suffered minor damages compared to the RC counterpart due to microcracking produced in it.
4. Compared with the RC models, the yield stiffness of the code-compliant and code-deficient models increased approximately 60% and 20% in the ECC models, respectively.
5. The computed R-Factor for the code-compliant RC and ECC-RC was approximately 7.5 and 12, respectively. These R-factor values are more significant than the code-specified value of 5, showing an increase of 50% and 140%, respectively. This increase in the R-factor

Fig. 9 Comparison of different dynamic response parameters of RC and ECC/RC specimens

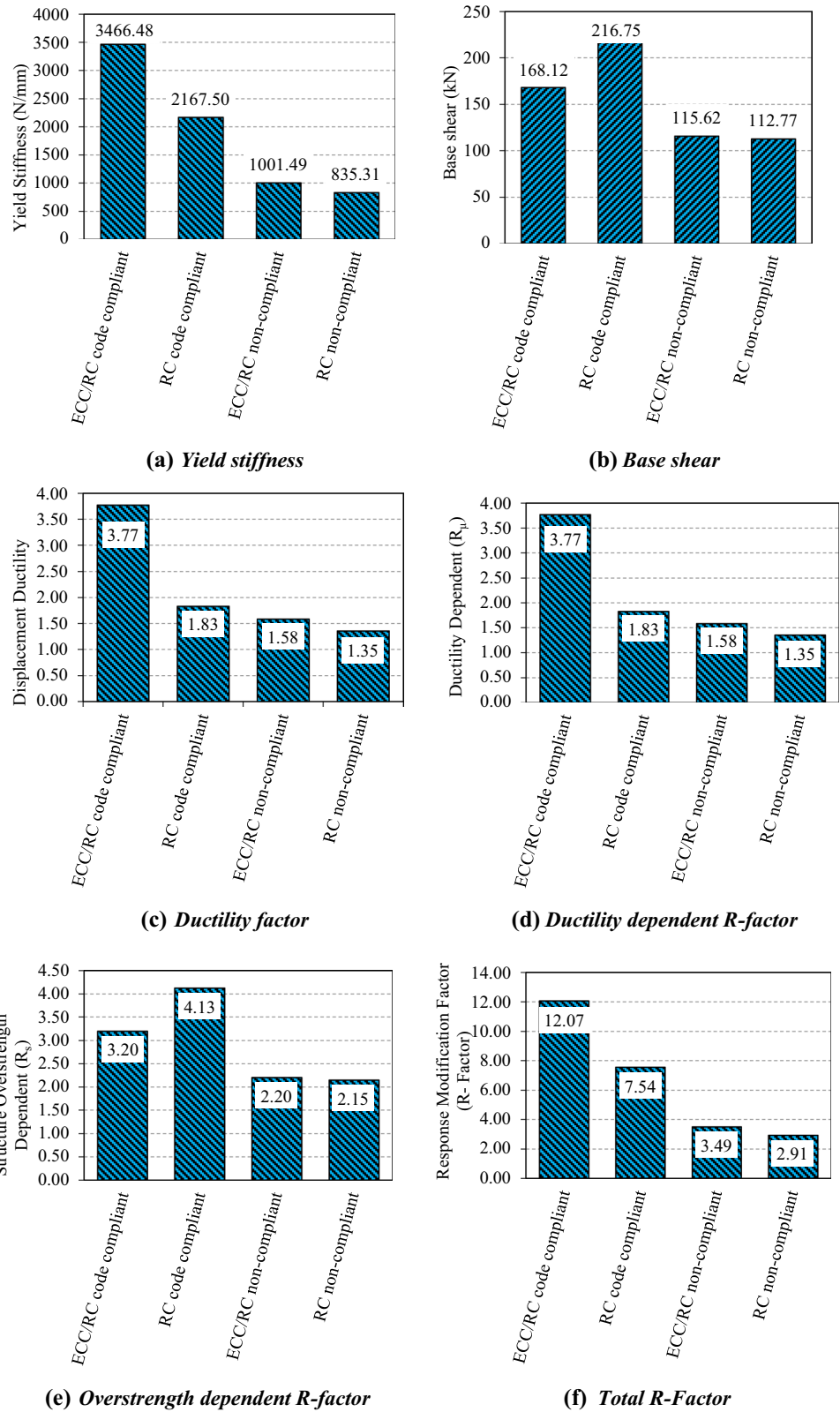
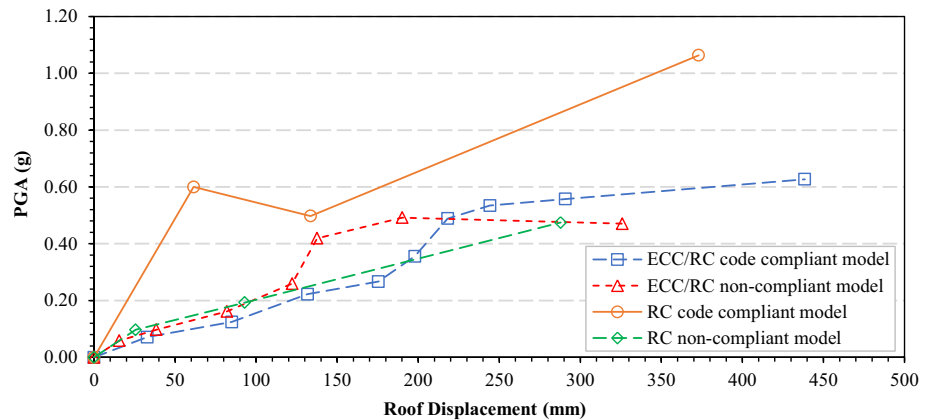


Table 5 Response modification factor (R-Factor) calculations

Model Configuration	Code compliant		Non-compliant	
	ECC/RC	RC	ECC/RC	RC
Yield stiffness, kip/in. (KN/m)	19.79 (3466.48)	12.38 (2167.5)	5.72 (1001.49)	4.77 (835.31)
Displacement ductility	3.77	1.83	1.58	1.35
Overstrength-based R_s factor	3.20	4.13	2.20	2.15
Time period, T (sec)	0.76	0.71	0.93	1.15
Ductility-based R_μ factor	3.77	1.83	1.58	1.35
Total R-factor, (approximate)	12.07 (12)	7.54 (7.5)	3.49 (3)	2.91 (2.5)

Fig. 10 Seismic response curves for the considered prototype structures

of ECC-RC frames may be attributed to the dissipating energy capacity of ECC in tension, and the maximum roof drifts displacement due to ductility higher values which caused the main effect on the R-factor.

6. The R-factor for code-deficient RC and ECC-RC models was approximately 2.9 and 3.5, respectively. However, compared with code-specified values, these R-factors, with all those structural deficiencies in RC and ECC-RC models, showed only a decrease of 42% and 30%, respectively. Therefore, a slight increase in the R-factor of the ECC-RC deficient model may indicate the energy dissipation and confining effect of the ECC fiber matrix.

Acknowledgements The authors would like to express their gratitude to Higher Education Commission (HEC), Pakistan, for funding the National Research Program for Universities. This paper's opinions, findings, and conclusions are the authors' opinions and do not necessarily reflect sponsors' views.

Data availability Some or all data, models, or codes that support the findings of this study are available from the corresponding author upon reasonable request. (Raw/Processed data, Model's Detailing, and material properties).

Compliance with ethical standards

Conflict of interest The authors declare that they have no known competing financial interests or personal relationships that could have influenced the work reported in this paper.

References

- Gencturk B, Hosseini F (2015) Evaluation of reinforced concrete and reinforced engineered cementitious composite (ECC) members and structures using small-scale testing. *Can J Civ Eng* 42:164–177. <https://doi.org/10.1139/cjce-2013-0445>
- Parra-Montesinos GJ, Peterfreund SW, Chao S-H (2005) Highly damage-tolerant beam-column joints through use of high-performance fiber-reinforced cement composites. *ACI Struct J* 102:487–495
- Yuan F, Pan J, Xu Z, Leung CKY (2013) A comparison of engineered cementitious composites versus normal concrete in beam-column joints under reversed cyclic loading. *Mater Struct* 46:145–159. <https://doi.org/10.1617/s11527-012-9890-6>
- Kam WY, Pampanin S (2011) The seismic performance of RC buildings in the 22 February 2011 Christchurch earthquake. *Struct Concr* 12:223–233. <https://doi.org/10.1002/suco.201100044>
- Westenenk B, de la Llera JC, Jünemann R et al (2013) Analysis and interpretation of the seismic response of RC buildings in Concepción during the February 27, 2010, Chile earthquake. *Bull Earthq Eng* 11:69–91. <https://doi.org/10.1007/s10518-012-9404-5>

6. Badrashi YI, Ali Q, Ashraf M, Rashid M (2016) Seismic design characterization of RC special moment resisting frames in pakistan-field survey to laboratory experiments. *J Eng Appl Sci* 35:25–32
7. Ghayeb HH, Abdul Razak H, Ramli Sulong NH (2020) Seismic performance of innovative hybrid precast reinforced concrete beam-to-column connections. *Eng Struct* 202:109886. <https://doi.org/10.1016/j.engstruct.2019.109886>
8. Joint ACI-ASCE Committee 352 (2002) Recommendations for Design of Beam-Column Connections in Monolithic Reinforced Concrete Structures (ACI-ASCE 352-02). Tech Rep 1–37
9. Jiuru T, Chaobin H, Kaijian Y, Yongcheng Y (1992) Seismic behavior and shear strength of framed joint using steel-fiber reinforced concrete. *J Struct Eng* 118:341–358
10. Sharma A, Reddy GR, Vaze KK (2012) Shake table tests on a non-seismically detailed RC frame structure. *Struct Eng Mech* 41:1–24
11. Saghafi MH, Shariatmadar H (2018) Enhancement of seismic performance of beam-column joint connections using high performance fiber reinforced cementitious composites. *Constr Build Mater* 180:665–680. <https://doi.org/10.1016/j.conbuildmat.2018.05.221>
12. Choi WC, Do YH, Cho CG, Feo L (2014) Attempts to apply high performance fiber-reinforced cement composite (HPFRCC) to infrastructures in South Korea. *Compos Struct* 109:211–223. <https://doi.org/10.1016/j.compstruct.2013.10.027>
13. Allawi AA, Ali SI (2020) Flexural behavior of composite GFRP pultruded I-section beams under static and impact loading. *Civ Eng J* 6:2143–2158. <https://doi.org/10.28991/cej-2020-03091608>
14. Balamuralikrishnan R, Saravanan J (2021) Effect of addition of alccofine on the compressive strength of cement mortar cubes. *Emerg Sci J* 5:155–170. <https://doi.org/10.28991/esj-2021-01265>
15. Jin Q, Li VC (2019) Structural and durability assessment of ECC/concrete dual-layer system for tall wind turbine towers. *Eng Struct* 196:109338. <https://doi.org/10.1016/j.engstruct.2019.109338>
16. Li VC, Fukuyama H, Mikame A (1998) Development of ductile engineered cementitious composite elements for seismic structural applications. In: Proceedings structural engineering world congress (SEWC), San Francisco
17. Deng K, Wang T, Kurata M et al (2018) Numerical study on a fully-prefabricated damage-tolerant beam to column connection for an earthquake-resilient frame. *Eng Struct* 159:320–331. <https://doi.org/10.1016/j.engstruct.2018.01.011>
18. Song JH, Lee ET, Eun HC (2020) Shear strength of reinforced concrete columns retrofitted by glass fiber reinforced polyurea. *Civ Eng J* 6:1852–1863. <https://doi.org/10.28991/cej-2020-03091587>
19. Chen B, Liu J (2005) Contribution of hybrid fibers on the properties of the high-strength lightweight concrete having good workability. *Cem Concr Res* 35:913–917. <https://doi.org/10.1016/j.cemconres.2004.07.035>
20. Ganesan N, Indira PV, Abraham R (2007) Steel fibre reinforced high performance concrete beam-column joints subjected to cyclic loading. *ISET J Earthq Technol* 44:445–456
21. Vasanelli E, Micelli F, Aiello MA, Plizzari G (2013) Crack width prediction of FRC beams in short and long term bending condition. *Mater Struct Constr* 47:39–54. <https://doi.org/10.1617/s11527-013-0043-3>
22. Di Prisco M, Plizzari G, Vandewalle L (2009) Fibre reinforced concrete: new design perspectives. *Mater Struct* 42:1261–1281. <https://doi.org/10.1617/s11527-009-9529-4>
23. Kim JK, Kim JS, Ha GJ, Kim YY (2007) Tensile and fiber dispersion performance of ECC (engineered cementitious composites) produced with ground granulated blast furnace slag. *Cem Concr Res* 37:1096–1105. <https://doi.org/10.1016/j.cemconres.2007.04.006>
24. Şahmaran M, Li VC (2009) Influence of microcracking on water absorption and sorptivity of ECC. *Mater Struct Constr* 42:593–603. <https://doi.org/10.1617/s11527-008-9406-6>
25. Shakya K, Watanabe K, Matsumoto K, Niwa J (2012) Application of steel fibers in beam-column joints of rigid-framed railway bridges to reduce longitudinal and shear rebars. *Constr Build Mater* 27:482–489. <https://doi.org/10.1016/j.conbuildmat.2011.07.016>
26. Shannag MJ, Barakat S, Abdul-Kareem M (2002) Cyclic behavior of HPFRCC-repaired reinforced concrete interior beam-column joints. *Mater Struct Constr* 35:348–356
27. Fischer G, Fukuyama H, C.Li V (2002) Effect of matrix ductility on the performance of reinforced ECC column members under reversed cyclic loading conditions. In: Proceedings of the JCI international Workshop on Ductile Fiber Reinforced Cementitious Composites (DFRCC)- Application and Evaluation. pp 269–278
28. Li VC, Wang S, Wu C (2001) Tensile strain-hardening behavior of polyvinyl alcohol engineered cementitious composite (PVA-ECC). *ACI Mater J* 98:483–492. <https://doi.org/10.14359/10851>
29. Ahmad N, Akbar J, Rizwan M et al (2019) Haunch retrofitting technique for seismic upgrading deficient RC frames. *Bull Earthquake Eng* 17:3895–3932. <https://doi.org/10.1007/s10518-019-00638-9>
30. Rizwan M, Ahmed N, Khan AN (2017) Seismic performance of SMRF compliant and non-compliant RC frames. *ACI Struct Mater J*. <https://doi.org/10.1007/s10895-012-1126-1>
31. Akbar J, Ahmad N, Alam B, Ashraf M (2018) Seismic performance of RC frames retrofitted with haunch technique seismic performance of RC frames retrofitted with haunch technique. *Struct Eng Mech* 67:1–8. <https://doi.org/10.12989/sem.2018.67.1.001>
32. Quintana-Gallo P, Pampanin S, Carr AJ, Bonelli P (2010) Shake table tests of under-designed RC frames for the seismic retrofit of buildings – design and similitude requirements of the benchmark specimen. In: New Zealand society of earthquake engineering Conference
33. Said SH, Abdul Razak H (2016) Structural behavior of RC engineered cementitious composite (ECC) exterior beam-column joints under reversed cyclic loading. *Constr Build Mater* 107:226–234. <https://doi.org/10.1016/j.conbuildmat.2016.01.001>
34. Qudah S, Maalej M (2014) Application of engineered cementitious composites (ECC) in interior beam-column connections for enhanced seismic resistance. *Eng Struct* 69:235–245. <https://doi.org/10.1016/j.engstruct.2014.03.026>
35. Zhao X, Wu YF, Leung AY, Lam HF (2011) Plastic hinge length in reinforced concrete flexural members. *Procedia Eng* 14:1266–1274. <https://doi.org/10.1016/j.proeng.2011.07.159>
36. Tomažević M (2000) Some Aspects of Experimental Testing of Seismic Behavior of Masonry Walls and Models of Masonry Buildings. *ISET J Earthq Technol* 37:101–117
37. Ali Q, Khan AN, Ashraf M et al (2013) Seismic performance of stone masonry buildings used in the Himalayan belt. *Earthq Spectra* 29:1159–1181. <https://doi.org/10.1193/091711EQS228M>
38. Ahmad N, Shahzad A, Rizwan M et al (2017) Seismic performance assessment of non-compliant SMRF-reinforced concrete frame: shake-table test study. *J Earthq Eng* 00:1–19. <https://doi.org/10.1080/13632469.2017.1326426>
39. Newmark NM, Hall WJ (1982) Earthquake spectra and design. Engineering Monographs on Earthquake Criteria, Structural Design, and Strong Motion Records, Earthquake Engineering Research Institute
40. Chopra AK (2012) Dynamics of Structures, Fourth Edi. Prentice Hall, One Lake Street, Upper Saddle River, NJ 07458